Express Polymer Letters Vol.16, No.7 (2022) 694–704
Available online at www.expresspolymlett.com
https://doi.org/10.3144/expresspolymlett.2022.51

Research article

Flexible and cracked polymer membrane for thermal-expansive reversible fuses using three-dimensional groove patterns

Byeongjo Ko[1], *Sanghun Shin*[1], *Hongyun So*[1,2*]

[1]Department of Mechanical Engineering, Hanyang University, 04763 Seoul, South Korea
[2]Institute of Nano Science and Technology, Hanyang University, 04763 Seoul, South Korea

Received 21 January 2022; accepted in revised form 27 March 2022

Abstract. In this study, a novel, facile, and cost-efficient manufacturing process for thermal-expansive reversible fuse (TRF) was demonstrated by using a cracked conductive layer on a flexible polymer with three-dimensional (3D) groove patterns. The current cut-off mechanism was demonstrated by the actuation of a thin membrane with a conductive layer of the TRF fabricated by a 3D-patterned mold and flexible polymer. When external heat was induced, the membrane of the TRF swelled, and the platinum-coated conductive layer was stretched, resulting in a current cut-off. In contrast, the membrane shrank, and the TRF was reconnected when the heat source was removed. The major cracks parallel to the 3D-printed patterns and minor cracks across the patterns were analyzed through the scanning electron microscope images. In addition, TRFs with pattern intervals of 250 μm (low resolution) and 100 μm (high resolution) were characterized by observing the current signal and expansion thickness of the membrane simultaneously to analyze the effect of actuation on the cut-off tendency. Finally, by applying the repetitive temperature profile between 35 °C and the cut-off temperature, the reversible performance of the TRFs was demonstrated by the cut-off and reconnection processes. These results can be applied to passive cooling systems of electronic devices to prevent overheating, which can affect the performance and durability of the device.

Keywords: *polymer membrane, reversible fuse, thermal expansion, 3D-printed patterns, actuation*

1. Introduction

The importance of thermal management systems has been highlighted in various industries such as automobiles [1], buildings [2], medical fields [3], and electrical/electronic devices [4]. Various studies have been conducted to solve thermal issues, such as constructing real-time temperature monitoring systems [5], cooling systems of devices using heat sinks [6], and current cut-off devices such as electrical switches and fuses [7–9]. Above all, the use of the fuses is efficient in restricting the overheating of electrical/electronic devices by breaking the circuit, thereby shutting down the supplied current.

Previous studies have reported methods for fabricating various types of fuses, such as reversible switches composed of graphene [7, 8], electro-explosion methods using conductive links [9], and polymeric positive temperature coefficient (PPTC) materials [10–14]. In particular, PPTC materials are reversible fuses composed of a non-conductive polymeric matrix and metal composite. Through the volume expansion of the polymeric matrix, the conductive links of the metal can be broken, thereby protecting the overheating of devices caused by abnormal overcurrent. They have been considered a suitable method for protecting electrical devices from overcharging and

*Corresponding author, e-mail: hyso@hanyang.ac.kr

overheating for these reasons. However, the cut-off mode (*i.e.*, rapid increase in electrical resistance) through bulk expansion only occurs when the device temperature reaches the melting point of the polymeric matrix. In addition, as the devices block the increase in current caused by Joule heating, it is difficult to inhibit the overheating of electrical devices in a system where a constant current and voltage are applied. Therefore, a novel and straightforward fabrication method is required to implement a current cut-off mechanism that can react to the temperature of the heat source even with constant electrical inputs to protect the operating devices and circuits from overheating.

Recently, owing to various applications, such as wearable sensors for health care monitoring [15, 16], battery management systems [17, 18], and soft electronic devices [19, 20], flexible electronic technology based on stretchable polymers has been investigated. Several methods have been studied to produce flexible conductive devices, including the use of conductive polymers [21, 22], mixing polymers with liquid metal, including Galinstan [23, 24], and conductive particles or nanowires such as Cu nanowires [25]. In addition, metal deposition onto flexible polymer surfaces by spraying [26], filling conductive inks using doctor blades [27], and metal sputtering methods [28, 29] have also been used. Among them, the metal sputtering method can create a uniform electrode on the surface of a polymer matrix or film. It can propagate cracks that increase the electrical sensitivity by the deformation of devices. However, it is well known that most stretchable polymers have poor thermal conductivity [30, 31] without mixing particles or conductive material coatings. To overcome this weakness, thermo-responsive polymer-based devices have been designed to actuate thin membranes depending on the temperature of the inner fluid and can be applied to micropumps or valves [32, 33].

Herein, a facile and rapid method of manufacturing reversible fuse is demonstrated using the actuation of an electrically conductive membrane and three-dimensional (3D) printing technology. Figure 1 depicts a schematic of the device concept of thermal-expansive reversible fuse (TRF). When an arbitrary heat source heats the TRF, the 3D-patterned thin polymer membrane swells, and the current drops, owing to its broken conductive link. In contrast, as the heat source is removed and the temperature decreases, the membrane contracts, and the current flows by reconnecting the electrode layer. TRFs are fabricated using a fused filament fabrication (FFF)-type 3D printer. The FFF-type 3D printer has a drawback: it leaves a specific pattern on the printed object due to continuously stacked filaments, which degrades its quality. Nevertheless, several studies have been conducted utilizing this disadvantage, such as hydrophobic surfaces [34], micro-drilling devices [35], and soft thermal actuators [36]. In this study, 3D patterns were used to increase the electrical sensitivity by implementing the patterns on a thin polymer membrane with conductive layer of TRF and aligning the cracks along with the 3D patterns.

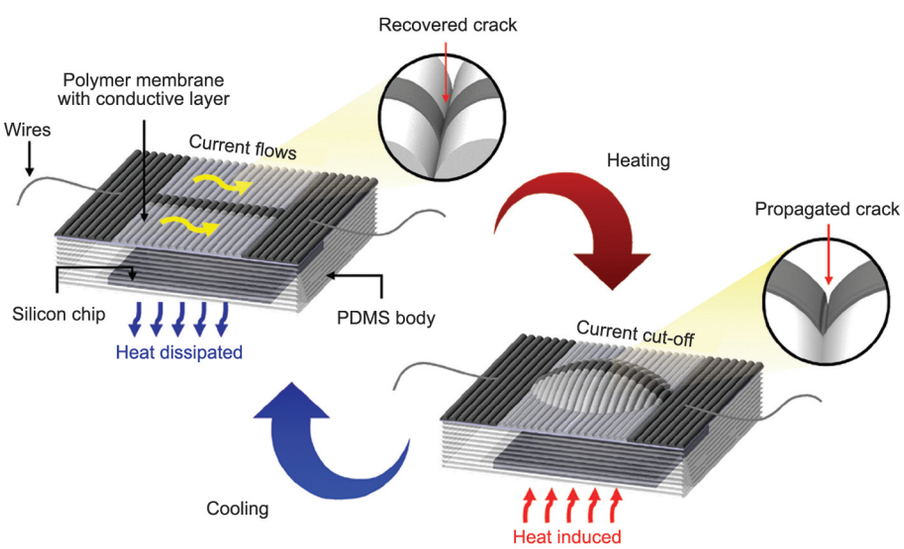

Figure 1. Schematic and operation principle of thermal-expansive reversible fuse (TRF) based on 3D-printed patterns. The polymer membrane of TRF actuates in response to external heat source reversibly.

Each TRF comprises three main parts: a square-shaped body with a cylindrical empty inner space (filled with air), a Pt electrode layer deposited on a thin polymer membrane with the 3D-printed patterns, and a silicon chip to facilitate heat transfer into the empty space of the body. The body was cast using a 3D-printed mold. In addition, the membrane mold was double-cast to apply the 3D patterns to the thin membrane. After integrating the body and membrane, a Pt conductive layer was deposited as an electrode onto the 3D-patterned membrane. Finally, each surface of the silicon chip and the bottom of the body were treated with oxygen plasma to bond together. The fabricated TRFs were preheated at high temperatures up to 150 °C to improve their sensitivity by generating cracks on the sputtered conductive layer. Subsequently, the current cut-off function of the TRFs was characterized by analyzing the current changes under discontinuous temperature conditions. In addition, the tendency of expansion thickness was characterized to demonstrate the effect of the actuation of the membrane at the same time. By repeated heating and cooling processes, the reversibility of the TRFs showed reliable performance with uniform current profiles at each temperature cycle. These results support the possibility of creating electro-thermal coupled systems with time-delay fuse [37] and passive cooling systems using a reversible cut-off process in response to external heat sources.

2. Manufacturing process

Figure 2 shows the overall fabrication procedure of the TRFs based on the 3D printing technology. The process was divided into four steps from Figure 2a to Figure 2d with sub-titles of each step: body, membrane mold, integrating, and preheating, respectively. As shown in Figure 2a, a body of the TRF was cast from the 3D-printed mold, which was printed using an FFF-type 3D printer (Guider IIs, Flashforge 3D Technology Ltd., Zhejiang, China) using polylactic acid (PLA) filament (diameter = 1.75 mm). The main body was designed to have a square shape of 15 mm with an empty cylindrical space with a diameter of 8 mm for the actuation of a thin membrane in response to external temperature. A polydimethylsiloxane (PDMS) mixture (prepolymer: curing agent = 10:1, Sylgard 184 Silicone Elastomer Kit, Dow Corning, Midland, Michigan, USA) was poured into the printed mold and baked in an oven (JSVO-60T, JS Research Inc., Gongju, South Korea) at 50 °C for 12 h, followed by separation of the cured body using a tweezer. As shown in Figure 2b, in order to acquire a membrane mold with groove patterns caused by stacked filament layers, the double casting method was applied by using ultraviolet (UV) curable resin (Sun Drop, hard type, PADICO, Tokyo, Japan) and PLA mold. In addition, the membrane thickness was fixed at 300 μm using 3D modeling. UV resin was poured into the PLA mold and cured using a UV lamp (S-SUV3365, Skycares, Kimpo, Korea) for 30 min to harden the resin perfectly. The resin mold was then detached by softening the PLA mold in an acetone bath for 1 h. Membrane molds were designed with two printing thicknesses: low and high resolution (250 and 100 μm, respectively) to characterize the effect of printing resolution on the cut-off performance of TRFs. Furthermore, flat-type membrane molds were also prepared with the same thickness using a PLA mold and a petri dish for manufacturing plain surfaces without 3D patterns. Figure 2c depicts the major process of fabricating TRFs in three detailed steps. Ecoflex 0050 (EcoFlex, Smooth-On Inc., Macungie, PA, USA) was selected as a suitable membrane material because of its outstanding flexibility [38]. Ecoflex was poured onto the resin membrane, followed by simply putting a body on the mixture, as shown in Figure $2c_1$. It was cured at 60 °C for 30 min in an oven to integrate the membrane and body. Figure $2c_2$ describes the method of depositing an electrode layer onto the membrane. The integrated body was placed in a Pt sputtering chamber (E-1045, Hitachi Ltd., Tokyo, Japan). The Pt layer was deposited using a PLA mask with a width of 2 mm to make the 'I'-shaped electrode of the TRFs, which can facilitate the current cut-off operation with a narrow electrode part when the membrane is actuated. Sputtering was conducted twice at 30 mA for 120 s to clarify the current cut-off with low electrical resistance caused by the thick electrode layer. Finally, the TRF body with a membrane was attached to a 10 mm × 10 mm silicon chip, which can assist the heat transfer to the inner air of the TRF owing to its high thermal conductivity. Oxygen plasma treatment combined the TRF body and silicon chip by increasing the adhesion between the two parts, thus, sealing the air. As the last step of fabrication, a preheating process was conducted to improve the sensitivity of the TRFs by decreasing the cut-off temperature via initially aligned cracks when the membrane actuated in response to the exposed external heat, as shown

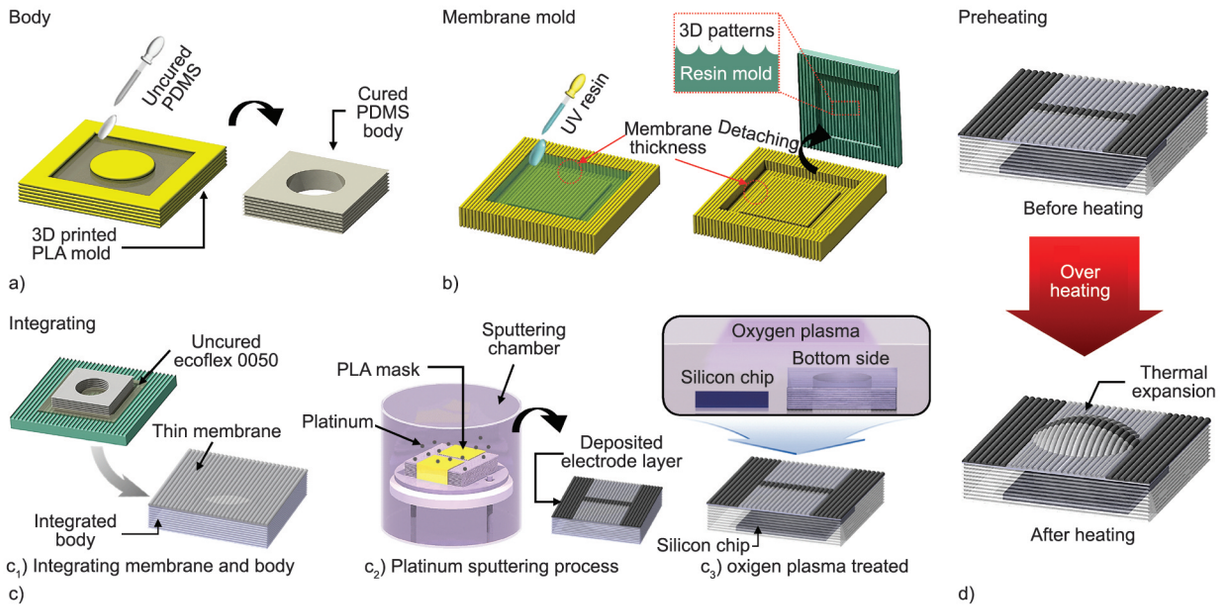

Figure 2. Overall fabrications of TRFs: (a) a PDMS body of the TRF cast by 3D-printed mold; (b) making UV resin-based 3D patterned membrane mold through double-casting method; (c) integrating processes of TRF: (c_1) integration of the thin membrane and the body, (c_2) deposition of Pt conductive layer onto the membrane, (c_3) bonding between the body and a 10 mm × 10 mm silicon chip by oxygen plasma treatment; (d) preheating process to initiate the cracks along with the 3D patterns.

in Figure 2d. Thus, the TRFs can cut the current off even with small actuation because of the created cracks on the conductive layer [39, 40]. For the preheating conditions, each TRF was overheated from 45 to 150 °C at intervals of 15 °C, showing an initial cut-off temperature of 105, 90, and 75 °C for TRFs with low-resolution, high-resolution, and flat membranes, respectively.

3. Experimental setup

Figure 3 illustrates the experimental setup to demonstrate the current cut-off performance of the TRFs. The fabricated device was placed on a metal block on the heating stage (HP-20D, DAIHAN Scientific, Wonju, Korea) with thermal grease. To prevent short circuits, electric wires were connected in series with an electrical load of 41 Ω. Additionally, PDMS supports were placed under the wires to reduce the thermal noise caused by the heating stage when the temperature was changed. The electrical output signal was monitored using a source meter (SMU 2614B, Keithley Instruments Ltd., Ohio, USA), connected to the TRF as a voltage supply. To analyze the tendency of the thermal expansion thickness of the TRF with current change depending on the induced temperature at the same time, an optical microscope (UM12,

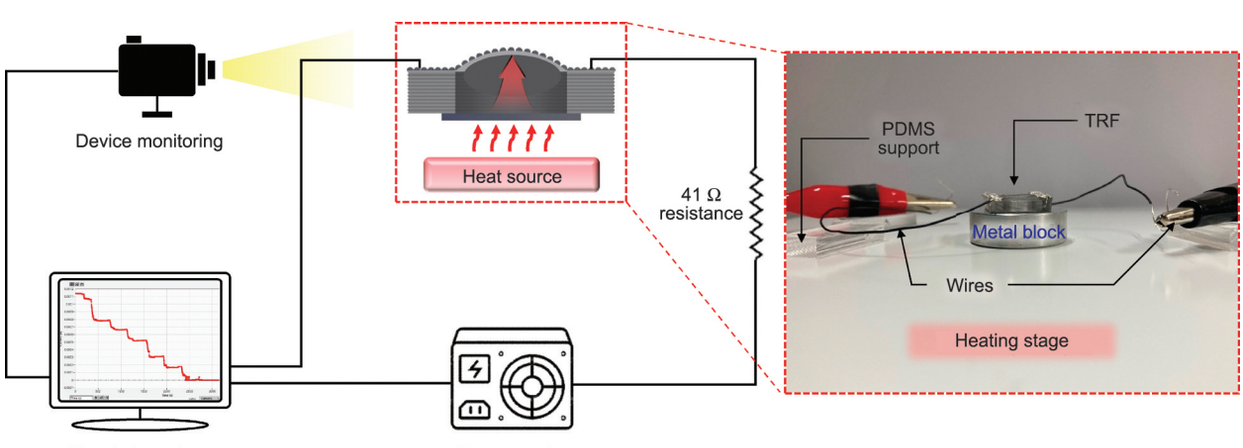

Figure 3. Schematic of the experimental setup for analyzing the characteristic of TRFs. Electrical signal and actuating behavior in response to the temperature change on the heating stage were monitored simultaneously.

ViTiny USA, USA) was also installed next to the heating stage.

4. Results and discussion

Figure 4 shows optical images of the membrane part of the TRFs. When the temperature of the heating stage increased, the thin polymer membrane with 3D patterns expanded (see Figures 4a and 4b). In addition, the top-view images of TRFs with low-resolution patterns, high-resolution patterns, and flat membranes were captured, as shown in Figures 4c, 4d, and 4e, respectively. Compared to the TRF with a flat membrane without 3D patterns (hereafter F-TRF), the TRF with low resolution showed a pattern width of 250 μm, and the TRF with a high resolution of 100 μm (hereafter, L-TRF and H-TRF, respectively). The 'I'-shaped electrode layer on the membrane was realized using a PLA mask to make a thin and conductive layer on the actuating part of the membrane, rapidly shutting the current down. It can be confirmed that the narrow part of the electrode was well aligned with the center of the inner empty space, which swells in response to the temperature increase. However, it should be noted that the F-TRF current was not restored to its initial value after the preheating process compared to the other types.

Scanning electron microscope (SEM) images of the normal and expanded states of each TRF were analyzed to compare the structure of the created cracks on the membrane through a preheating process. The states of L-TRF, H-TRF, and F-TRF before preheating are shown in Figures 5a, 5b, and 5c, respectively, whereas those of L-TRF, H-TRF, and F-TRF after preheating are presented in Figures 5d, 5e, and 5f, respectively. The pattern gap of L- and H-TRF were 247.23 and 102.61 mm, respectively, measured by the image analysis program. The cracks of each TRF propagated in all directions because of the axisymmetric expansion of the membrane. However, in the case of TRFs with 3D patterns on the membranes, cracks were generated mainly in two directions, parallel and vertical, to the patterns (hereafter, major cracks and minor cracks, respectively). In particular, major cracks were discovered in the valley of the groove patterns, which can significantly affect the current cut-off by breaking the electrical paths, as shown in Figures 5d and 5e. However, as seen in Figure 5f, cracks of F-TRF appeared irregularly

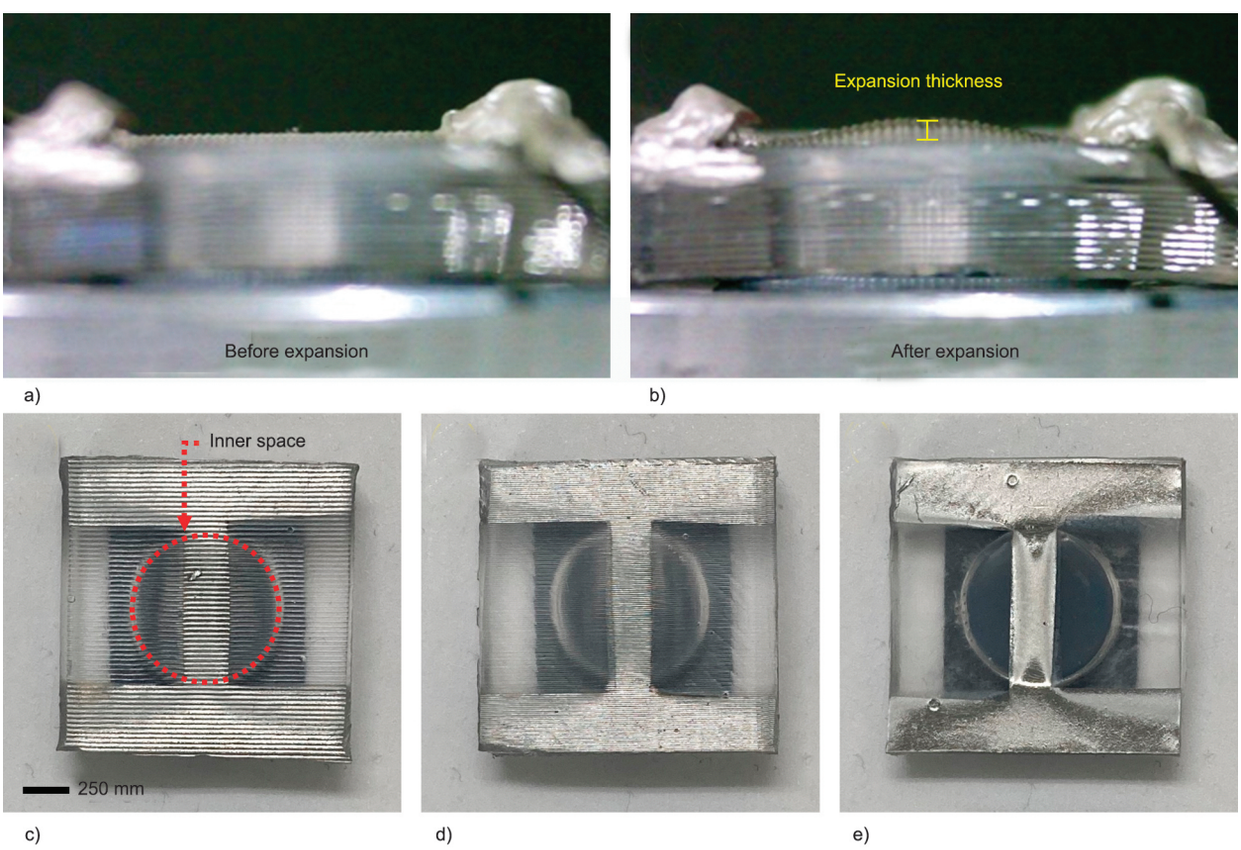

Figure 4. Optical images of the TRF during actuating process (a) before and (b) after expansion of membrane, and top view of each patterned TRF: (c) L-TRF, (d) H-TRF, and (e) F-TRF.

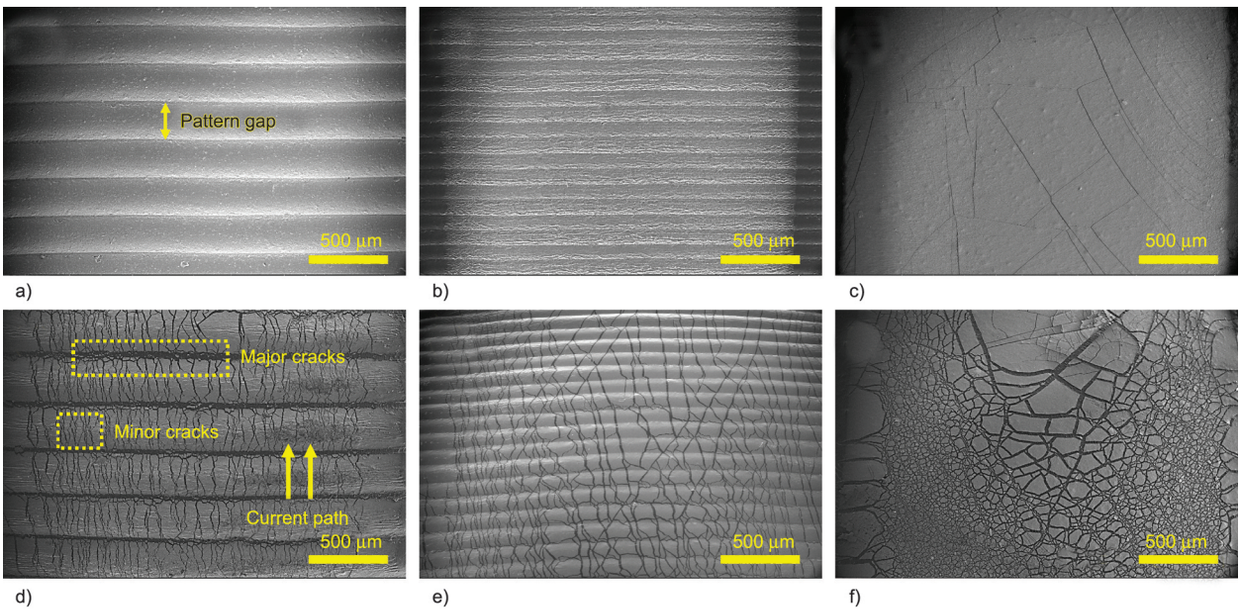

Figure 5. SEM images of preheated TRFs to observe crack propagation: (a) before and (d) after expansion of L-TRF, (b) before and (e) after expansion of H-TRF, (c) before and (f) after expansion of F-TRF.

because the membrane of F-TRF had no guideline to align cracks, restricting the reconnection of the electrode metal during repeated actuation.

To demonstrate the tendency of crack propagation on the polymer membrane, the modulus of each pure membrane was further measured using a tensile tester (MCT-2150, AND Inc., Seoul, Korea), as shown in Figure 6a. Each type of membrane of TRF was prepared by using the square resin mold with a width of 15 mm and thickness of 300 μm. The measurement was conducted in two directions (*i.e.*, major and minor, as shown in Figure 5d). As a result, both membranes of L- and H-TRF showed the same tendency that the modulus along major direction was less than that along the minor direction (5.78 kPa difference for L-TRF and 4.96 kPa difference for H-TRF, as shown in Figure 6b), indicating the anisotropic cracks propagation along the valley of 3D groove patterns. In the case of F-TRF (*i.e.*, isotropic membrane), however, there was no distinct difference in the modulus with respect to the direction, demonstrating the effect of 3D groove patterns on anisotropic mechanical properties or behaviors [36, 41].

To characterize the cut-off mechanism of TRFs in response to the change in ambient temperature, two experiments were conducted using L- and H-TRF because F-TRF had no current flow after preheating owing to the irregular crack structure (see Figure 5f). Figure 7 shows the tendencies of the current changes and expansion thickness of the two TRFs depending on the temperature during the heating step. The tests were repeated five times to obtain reliable data. The

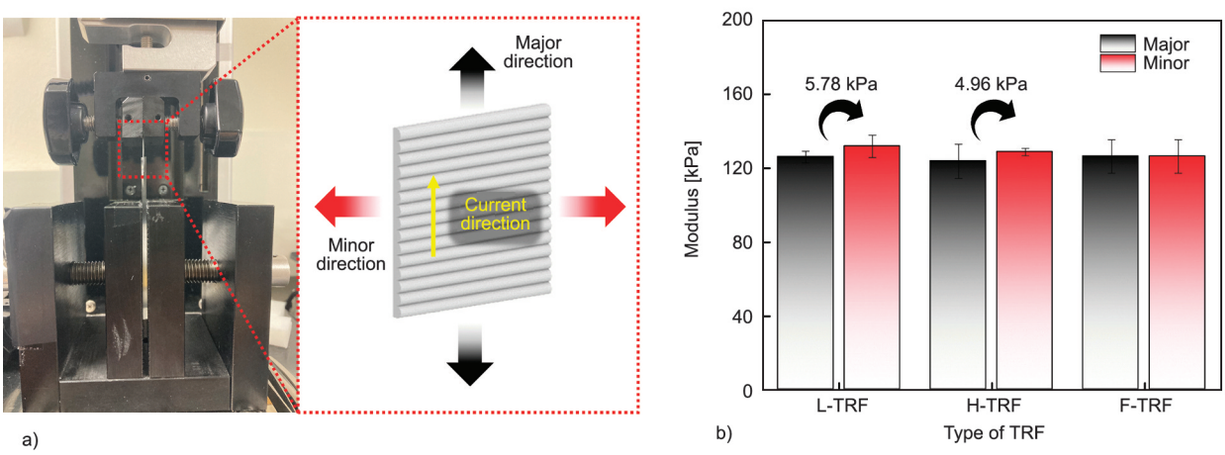

Figure 6. Measurement of membrane modulus. (a) tensile test setup and the measured directions and (b) modulus of pure membrane along with both directions with respect to the type of TRFs.

boundary of the sky blue and yellow areas indicates the cut-off point. In addition, the temperature was changed from 35 to 75 °C at intervals of 5 °C and maintained for 5 min to measure the saturated current and expansion thickness at each step. To accurately compare each current signal, the normalized current was calculated using the Equation (1):

$$Normalized\ current = \frac{I_s - I_0}{I_0} \quad (1)$$

where I_s is the saturated current at each temperature step, and I_0 is the current at room temperature without heating. This indicates that if the normalized current approaches –1, the current is shut down as I_s converges to zero when the temperature and actuated thermal expansion thickness increase. The normalized current decreased with an increase in the expansion thickness as the temperature increased. As shown in Figures 7a and 7b, both L- and H-TRF showed nonlinear profiles compared to the linear declination of general Pt metal. This indicates that the current decrease was accelerated owing to the actuation effect of the crack-based thin polymer membrane until the cut-off occurred. As a result, the cut-off temperature of L- and H-TRF was approximately 62.6 and 58.4 °C, respectively. In addition, the corresponding expansion thicknesses were evaluated as 0.533 and 0.616 mm for L-TRF and H-TRF, respectively. Although the cut-off temperature of L-TRF was higher than that of H-TRF, it could cut the current off by smaller actuation than H-TRF, showing a 0.083 mm lower expansion thickness due to more propagated major cracks, as shown in Figures 5d and 5e.

Finally, to demonstrate the reversibility of the TRFs, repetitive heating and cooling tests were performed. Figure 8 shows the transient test for representing the reversibility performance of the TRFs with the temperature cycle. The L-TRF was tested at temperatures between 35 and 65 °C, slightly higher than the cut-off temperature of L-TRF (*i.e.*, 62.6 °C), as shown in Figure 8a. As shown in Figure 8b, the H-TRF was tested at temperatures between 35 and 60 °C, which was slightly higher than the cut-off temperature of H-TRF (*i.e.*, 58.4 °C). The test conditions were started at room temperature, and six temperature cycles were repeated, followed by returning to room temperature. To measure the saturated current value, the heating step was maintained for 180 s. In comparison, the cooling time was 210 s, considering a slower recovery rate than the response rate. Both resolutions of the TRFs showed uniform electrical signals at each cycle.

Figure 9 shows the change of cracks during the reversibility test at a temperature of 35 °C (the temperature at which cracks initiated evidently), cut-off temperature (65 °C for L-TRF and 60 °C for H-TRF), and 25 °C (fully cooled temperature), as seen in Figure 8. To characterize the structural change of cracks during the reversibility cycle test, crack density at each temperature was analyzed using detailed SEM images and an image analysis program. The crack density was calculated as a ratio of crack area to the overall area of the acquired SEM image in this study. As a result, the crack density of approximately 6.98 and 7.90% was calculated at 35 °C for L-TRF and H-TRF, respectively. As the temperature increased

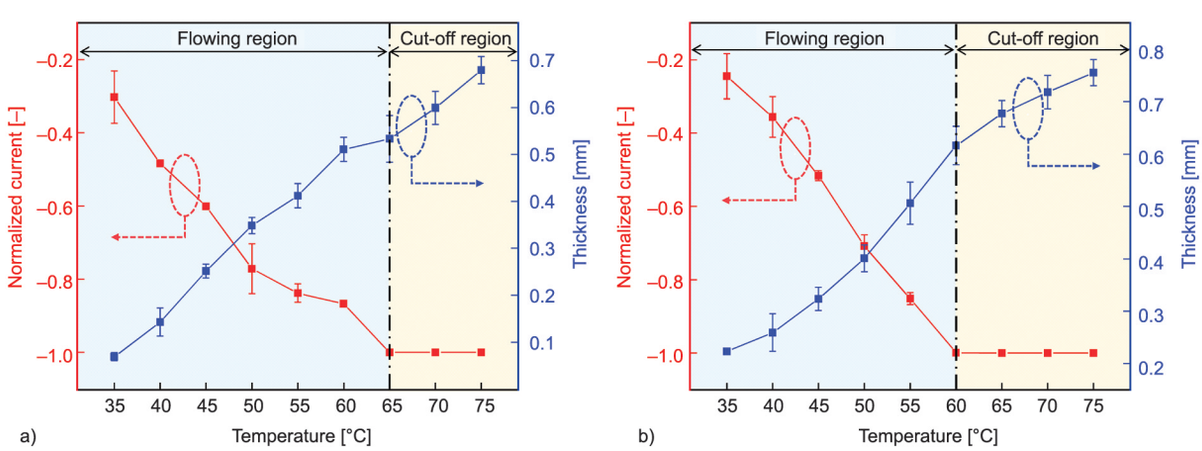

Figure 7. The tendency of electrical current flow and thermal expansion thickness with respect to the temperature. Both (a) L-TRF and (b) H-TRF show the current decreased as the thermal expansion thickness of the membrane increased by actuating motion.

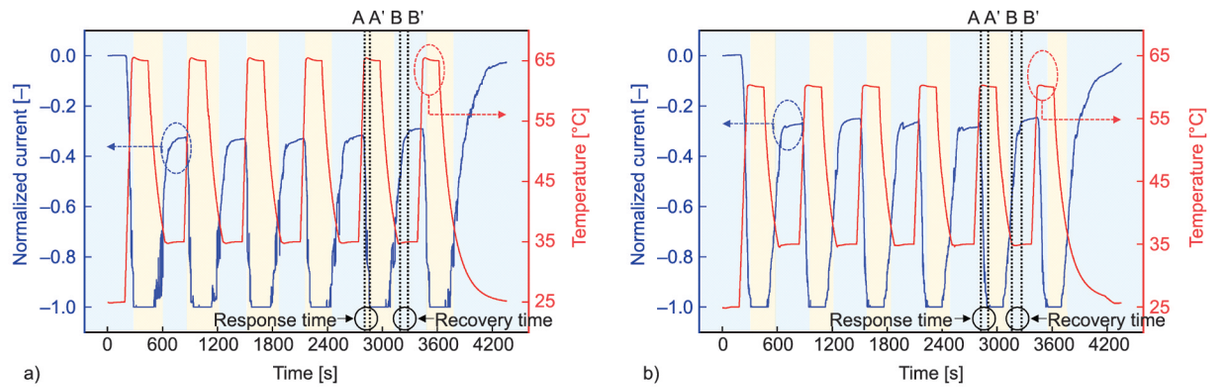

Figure 8. Repeated heating and cooling test to demonstrate the reversibility of the TRFs. (a) L-TRF and (b) H-TRF showed uniform electrical profiles at each temperature interval, from 35 °C to cut-off temperature.

to the cut-off temperature, the crack density increased to 12.02 and 14.81% for L-TRF and H-TRF, respectively. Thus, this increased crack density could cut the current off as the temperature increased. It was noteworthy that the propagated cracks became narrow (recovered) as the temperature returned to 25 °C, allowing the reflow of the current by the reconnection of the conductive layer. This analysis demonstrated the reliability and reversibility of TRF mechanisms.

Table 1 shows the average response and recovery times for both TRFs to characterize the sensitivity. Response time was defined as the time between the beginning of the cut-off temperature and the start of the cut-off operation (from line A to A′ in Figures 8a and 8b). In contrast, the recovery time was measured from 35 °C, which was the cooling temperature to the start point of current saturation (from line B to B′ in Figures 8a and 8b). According to the calculated results, the L-TRF exhibited much shorter response and recovery times than the H-TRF. The L-TRF responded to an external heat source at 37.4 s (1.37 times faster than H-TRF) and recovered in 65.8 s (1.12 times faster than H-TRF). It is noteworthy that the response and recovery time can be reduced by adjusting the thickness of the membrane or heating rate induced by the TRFs [42, 43]. This demonstrates that the cracks of L-TRF along the valley of 3D patterns were more aligned than those of H-TRF, as seen in the SEM images in Figures 5d and 5e. This shows that the major cracks parallel to the 3D patterns played an essential role in the cut-off process by breaking the Pt electrode easily in response to membrane actuation. These results demonstrate the

Table 1. Average response and recovery time of the TRFs during reversibility test.

	Response time [s]	Recovery time [s]
L-TRF (250 μm)	37.4±23.5	65.8±6.6
H-TRF (100 μm)	51.2±21.8	74.0±19.0

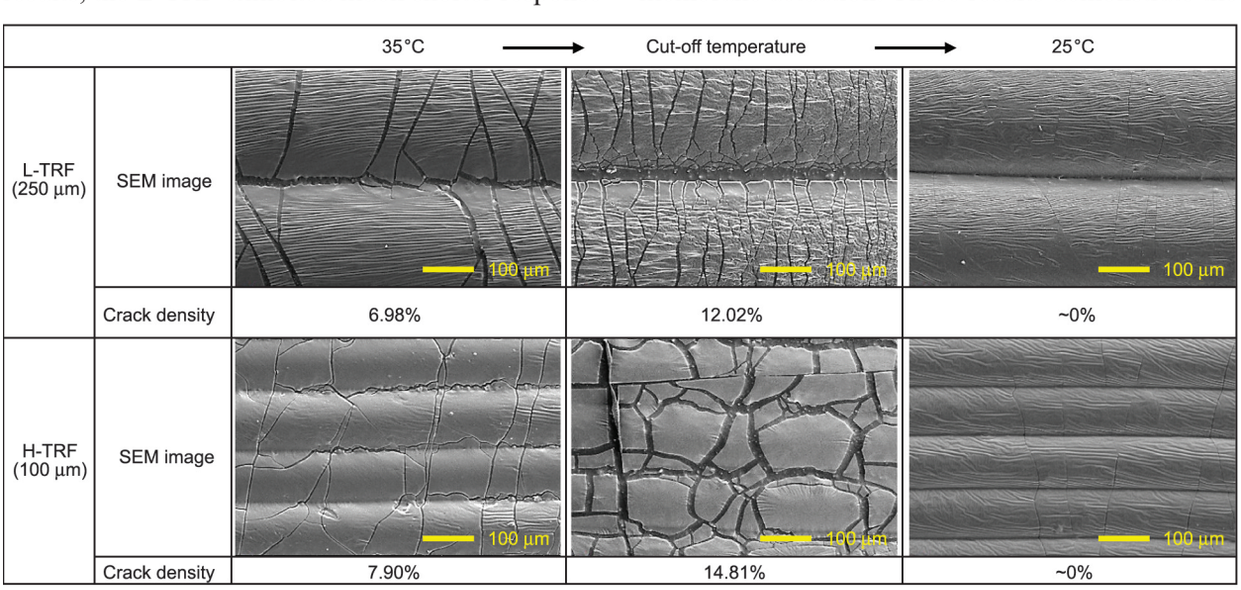

Figure 9. Crack propagation and corresponding crack density during reversibility cycle test.

function of thermal-expansive reversible fuse assisted by actuation of the membrane based on continuous 3D groove patterns, which can serve as a guideline for crack formation.

5. Conclusions

We investigated a novel and straightforward fabrication process for thermal-expansive reversible fuse (TRF) based on 3D groove patterns caused by stacked filaments of FFF-type 3D printing technology. Three types of TRFs were fabricated to characterize the performance of the TRFs depending on the width of the printing patterns. The membrane of TRF with 3D groove patterns was sputtered by Pt metal using an 'I'-shaped PLA mask. The narrow part of the electrode was stretched during the preheating process at high temperatures up to 150 °C, thereby creating cracks mainly in two directions, parallel and vertical, to 3D patterns. In particular, the parallel cracks generated along the valley of the patterns exhibited a significant role in the current cut-off function by improving the electrical sensitivity of the TRFs caused by the temperature change. The flat type of TRF (without 3D printing patterns) showed unsorted (irregular) crack propagation due to the absence of the 3D patterns as a guideline for crack generation, resulting in no reconnection of the electrode after the preheating process. Based on the fabricated devices, the performances of the TRFs were demonstrated by measuring the change in current and thermal expansion thickness with respect to the induced temperature. The L-TRF (printing resolution of 250 μm) showed a more sensitive cut-off response with a small actuation of 0.533 mm, despite a 5 °C higher cut-off temperature than H-TRF (printing resolution of 100 μm). Moreover, the reversibility of the TRFs was demonstrated by cycle tests between 35 °C and the cut-off temperature with uniform repeated current signal output. Finally, the L-TRF exhibited a higher electrical response to the temperature change with 37.4 s of response time (1.36 times faster than H-TRF) and 65.8 s of recovery time (1.12 times faster than H-TRF). This study supports the additive manufacturing-assisted method of constructing a passive current cut-off system for thermal management systems such as time-delay circuit breakers of electro-thermal coupled systems.

Acknowledgements

This work was supported by the Korea Institute of Energy Technology Evaluation and Planning (KETEP), and the Ministry of Trade, Industry, & Energy (MOTIE) of the Republic of Korea (No. 20212020800090).

References

[1] Oh S. K., Lundh J. S., Shervin S., Chatterjee B., Lee D. K., Choi S., Kwak J. S., Ryou J-H.: Thermal management and characterization of high-power wide-bandgap semiconductor electronic and photonic devices in automotive applications. Journal of Electronic Packaging, **141**, 020801 (2019). https://doi.org/10.1115/1.4041813

[2] Elnajjar E.: Using PCM embedded in building material for thermal management: Performance assessment study. Energy and Buildings, **151**, 28–34 (2017). https://doi.org/10.1016/j.enbuild.2017.06.010

[3] Xiong S-W., Zhang P., Xia Y., Fu P-G., Gai J-G.: Antimicrobial hexagonal boron nitride nanoplatelet composites for the thermal management of medical electronic devices. Materials Chemistry Frontiers, **3**, 2455–2462 (2019). https://doi.org/10.1039/C9QM00411D

[4] Ghahfarokhi P. S., Podgornovs A., Kallaste A., Cardoso A. J. M., Belahcen A., Vaimann T., Tiismus H., Asad B.: Opportunities and challenges of utilizing additive manufacturing approaches in thermal management of electrical machines. IEEE Access, **9**, 36368–36381 (2021). https://doi.org/10.1109/ACCESS.2021.3062618

[5] Youn D-Y., Jung U., Naqi M., Choi S-J., Lee M-G., Lee S., Park H-J., Kim I-D., Kim S.: Wireless real-time temperature monitoring of blood packages: Silver nanowire-embedded flexible temperature sensors. ACS Applied Materials and Interfaces, **10**, 44678–44685 (2018). https://doi.org/10.1021/acsami.8b11928

[6] Kalbasi R.: Introducing a novel heat sink comprising PCM and air – Adapted to electronic device thermal management. International Journal of Heat and Mass Transfer, **169**, 120914 (2021). https://doi.org/10.1016/j.ijheatmasstransfer.2021.120914

[7] Standley B., Bao W., Zhang H., Bruck J., Lau C. N., Bockrath M.: Graphene-based atomic-scale switches. Nano Letters, **8**, 3345–3349 (2008). https://doi.org/10.1021/nl801774a

[8] Pearson A. C., Jamieson S., Linford M. R., Lunt B. M., Davis R. C.: Oxidation of graphene 'bow tie' nanofuses for permanent, write-once-read-many data storage devices. Nanotechnology, **24**, 135202 (2013). https://doi.org/10.1088/0957-4484/24/13/135202

[9] Ding X., Lou W., Feng Y.: A controllable IC-compatible thin-film fuse realized using electro-explosion. AIP Advances, **6**, 015316 (2016). https://doi.org/10.1063/1.4941074

[10] Yang R., Wang Y., Wu D., Deng Y., Luo Y., Cui X., Wang X., Shu Z., Yang C.: Low-temperature fusible silver micro/nanodendrites-based electrically conductive composites for next-generation printed fuse-links. ACS Nano, **11**, 7710–7718 (2017). https://doi.org/10.1021/acsnano.7b00935

[11] Zhang X., Zheng S., Zheng X., Liu Z., Yang W., Yang M.: Distinct positive temperature coefficient effect of polymer–carbon fiber composites evaluated in terms of polymer absorption on fiber surface. Physical Chemistry Chemical Physics, **18**, 8081–8087 (2016). https://doi.org/10.1039/C6CP00398B

[12] Liu Y., Asare E., Porwal H., Barbieri E., Goutianos S., Evans J., Newton M., Busfield J. J. C., Peijs T., Zhang H., Bilotti E.: The effect of conductive network on positive temperature coefficient behaviour in conductive polymer composites. Composites Part A: Applied Science and Manufacturing, **139**, 106074 (2020). https://doi.org/10.1016/j.compositesa.2020.106074

[13] Zha J-W., Li W-K., Liao R-J., Bai J., Dang Z-M.: High performance hybrid carbon fillers/binary–polymer nanocomposites with remarkably enhanced positive temperature coefficient effect of resistance. Journal of Materials Chemistry A, **1**, 843–851 (2013). https://doi.org/10.1039/C2TA00429A

[14] Zhang X., Zheng X., Ren D., Liu Z., Yang W., Yang M.: Unusual positive temperature coefficient effect of polyolefin/carbon fiber conductive composites. Materials Letters, **164**, 587–590 (2016). https://doi.org/10.1016/j.matlet.2015.11.077

[15] Oh S. Y., Hong S. Y., Jeong Y. R., Yun J., Park H., Jin S. W., Lee G., Oh J. H., Lee H., Lee S-S., Ha J. S.: Skin-attachable, stretchable electrochemical sweat sensor for glucose and pH detection. ACS Applied Materials and Interfaces, **10**, 13729–13740 (2018). https://doi.org/10.1021/acsami.8b03342

[16] Yang H., Gong L. H., Zheng Z., Yao X. F.: Highly stretchable and sensitive conductive rubber composites with tunable piezoresistivity for motion detection and flexible electrodes. Carbon, **158**, 893–903 (2020). https://doi.org/10.1016/j.carbon.2019.11.079

[17] Meng Y., Wu H., Zhang Y., Wei Z.: A flexible electrode based on a three-dimensional graphene network-supported polyimide for lithium-ion batteries. Journal of Materials Chemistry A, **2**, 10842–10846 (2014). https://doi.org/10.1039/C4TA00364K

[18] Cha H., Kim J., Lee Y., Cho J., Park M.: Issues and challenges facing flexible lithium-ion batteries for practical application. Small, **14**, 1702989 (2018). https://doi.org/10.1002/smll.201702989

[19] Cao J., Qin L., Liu J., Ren Q., Foo C. C., Wang H., Lee H. P., Zhu J.: Untethered soft robot capable of stable locomotion using soft electrostatic actuators. Extreme Mechanics Letters, **21**, 9–16 (2018). https://doi.org/10.1016/j.eml.2018.02.004

[20] Li P., Wang Y., Gupta U., Liu J., Zhang L., Du D., Foo C. C., Ouyang J., Zhu J.: Transparent soft robots for effective camouflage. Advanced Functional Materials, **29**, 1901908 (2019). https://doi.org/10.1002/adfm.201901908

[21] Nambiar S., Yeow J. T. W.: Conductive polymer-based sensors for biomedical applications. Biosensors and Bioelectronics, **26**, 1825–1832 (2011). https://doi.org/10.1016/j.bios.2010.09.046

[22] Lee I., Kim G. W., Yang M., Kim T-S.: Simultaneously enhancing the cohesion and electrical conductivity of PEDOT:PSS conductive polymer films using DMSO additives. ACS Applied Materials and Interfaces, **8**, 302–310 (2016). https://doi.org/10.1021/acsami.5b08753

[23] Ling K., Kim K., Lim S.: Flexible liquid metal-filled metamaterial absorber on polydimethylsiloxane (PDMS). Optics Express, **23**, 21375 (2015). https://doi.org/10.1364/OE.23.021375

[24] Oh J. H., Woo J. Y., Jo S., Han C-S.: Pressure-conductive rubber sensor based on liquid-metal-PDMS composite. Sensors and Actuators A: Physical, **299**, 111610 (2019). https://doi.org/10.1016/j.sna.2019.111610

[25] Wang R., Ruan H.: Synthesis of copper nanowires and its application to flexible transparent electrode. Journal of Alloys and Compounds, **656**, 936–943 (2016). https://doi.org/10.1016/j.jallcom.2015.09.279

[26] Kim S., Oh S., Jung Y., Moon H., Lim H.: Customizable, flexible pressure, and temperature step sensors with human skinlike color. ACS Omega, **3**, 1110–1116 (2018). https://doi.org/10.1021/acsomega.7b01868

[27] Nie B., Li X., Shao J., Li X., Tian H., Wang D., Zhang Q., Lu B.: Flexible and transparent strain sensors with embedded multiwalled carbon nanotubes meshes. ACS Applied Materials and Interfaces, **9**, 40681–40689 (2017). https://doi.org/10.1021/acsami.7b12987

[28] Tang J., Guo H., Zhao M., Yang J., Tsoukalas D., Zhang B., Liu J., Xue C., Zhang W.: Highly stretchable electrodes on wrinkled polydimethylsiloxane substrates. Scientific Reports, **5**, 16527 (2015). https://doi.org/10.1038/srep16527

[29] Jang H. Y., Lee S-K., Cho S. H., Ahn J-H., Park S.: Fabrication of metallic nanomesh: Pt nano-mesh as a proof of concept for stretchable and transparent electrodes. Chemistry of Materials, **25**, 3535–3538 (2013). https://doi.org/10.1021/cm402085k

[30] Song J., Peng Z., Zhang Y.: Enhancement of thermal conductivity and mechanical properties of silicone rubber composites by using acrylate grafted siloxane copolymers. Chemical Engineering Journal, **391**, 123476 (2020). https://doi.org/10.1016/j.cej.2019.123476

[31] Si W., He X., Huang Y., Gao X., Zheng X., Zheng X., Leng C., Su F., Wu D.: Polydimethylsiloxane/aluminum oxide composites prepared by spatial confining forced network assembly for heat conduction and dissipation. RSC Advances, **8**, 36007–36014 (2018). https://doi.org/10.1039/C8RA07229A

[32] Cai Z., Xiang J., Chen H., Wang W.: Membrane-based valves and inward-pumping system for centrifugal microfluidic platforms. Sensors and Actuators B: Chemical, **228**, 251–258 (2016). https://doi.org/10.1016/j.snb.2015.12.049

[33] Takao H., Miyamura K., Ebi H., Ashiki M., Sawada K., Ishida M.: A MEMS microvalve with PDMS diaphragm and two-chamber configuration of thermo-pneumatic actuator for integrated blood test system on silicon. Sensors and Actuators A: Physical, **119**, 468–475 (2005). https://doi.org/10.1016/j.sna.2004.10.023

[34] Kang B., Sung J., So H.: Realization of superhydrophobic surfaces based on three-dimensional printing technology. International Journal of Precision Engineering and Manufacturing-Green Technology, **8**, 47–55 (2021). https://doi.org/10.1007/s40684-019-00163-9

[35] Park S., Ko B., Lee H., So H.: Rapid manufacturing of micro-drilling devices using FFF-type 3D printing technology. Scientific Reports, **11**, 12179 (2021). https://doi.org/10.1038/s41598-021-91149-8

[36] Shin S., So H.: Time-dependent motion of 3D-printed soft thermal actuators for switch application in electric circuits. Additive Manufacturing, **39**, 101893 (2021). https://doi.org/10.1016/j.addma.2021.101893

[37] Shu L., Guo L., Wu G-C., Chen W.: Research of thermal protection characteristics for circuit breakers considering nonlinear electro-thermal-structural coupling. Applied Thermal Engineering, **153**, 85–94 (2019). https://doi.org/10.1016/j.applthermaleng.2019.02.068

[38] Zhao Y., Yang W., Tan Y. J., Li S., Zeng X., Liu Z., Tee B. C-K.: Highly conductive 3D metal-rubber composites for stretchable electronic applications. APL Materials, **7**, 031508 (2019). https://doi.org/10.1063/1.5083942

[39] Wang S., Xiao P., Liang Y., Zhang J., Huang Y., Wu S., Kuo S-W., Chen T.: Network cracks-based wearable strain sensors for subtle and large strain detection of human motions. Journal of Materials Chemistry C, **6**, 5140–5147 (2018). https://doi.org/10.1039/C8TC00433A

[40] Yang T., Li X., Jiang X., Lin S., Lao J., Shi J., Zhen Z., Li Z., Zhu H.: Structural engineering of gold thin films with channel cracks for ultrasensitive strain sensing. Materials Horizons, **3**, 248–255 (2016). https://doi.org/10.1039/C6MH00027D

[41] Lee H. M., Sung J., Ko B., Lee H., Park S., So H., Yoon G. H.: Modeling and application of anisotropic hyperelasticity of PDMS polymers with surface patterns obtained by additive manufacturing technology. Journal of the Mechanical Behavior of Biomedical Materials, **118**, 104412 (2021). https://doi.org/10.1016/j.jmbbm.2021.104412

[42] Zhang W., Aljasem K., Zappe H., Seifert A.: Completely integrated, thermo-pneumatically tunable microlens. Optics Express, **19**, 2347–2362 (2011). https://doi.org/10.1364/OE.19.002347

[43] Kwon H-J., Lee S. W., Lee S. S.: Braille dot display module with a PDMS membrane driven by a thermopneumatic actuator. Sensors and Actuators A: Physical, **154**, 238–246 (2009). https://doi.org/10.1016/j.sna.2008.10.002